# Supporting Information

## Exploiting Solid-State Dynamic Nuclear Polarization NMR Spectroscopy to Establish the Spatial Distribution of Polymorphic Phases in a Solid Material

Samuel F. Cousin,[a] Colan E. Hughes,[b] Fabio Ziarelli,[c] Stéphane Viel,[a] Giulia Mollica,*[a] Kenneth D. M. Harris,*[b] Arthur C. Pinon*[d] and Pierre Thureau*[a]

[a] Dr S. F. Cousin, Dr G. Mollica, Prof. S. Viel, Dr P. Thureau
Aix Marseille Univ, CNRS, ICR, Marseille, France.
E-mails: giulia.mollica@univ-amu.fr and pierre.thureau@univ-amu.fr
[b] Dr C. E. Hughes, Prof. Kenneth D. M. Harris
School of Chemistry, Cardiff University, Park Place, Cardiff CF10 3AT, Wales, United Kingdom.
E-mail: harriskdm@cardiff.ac.uk
[c] Dr F. Ziarelli
Aix Marseille Univ, CNRS, Centrale Marseille, FSCM, Marseille, France.
[d] Dr A. C. Pinon
Swedish NMR Center, University of Gothenburg, Gothenburg, SE-405 30, Sweden.
E-mail: arthur.pinon@gu.se

## 1. Sample Characterization

### 1.1 Powder XRD Studies of Powder Samples of Form I of m-ABA Following Impregnation with Solutions Containing the TEKPol and AMUPol Polarizing Agents

Following impregnation of a freshly prepared powder sample of Form I of *m*-ABA with a solution containing TEKPol in 1,1,2,2-tetrachloroethane (as described in Section 1.1.2), powder XRD data were recorded in two separate experiments using a Bruker D8 instrument operating in transmission mode using CuK$\alpha_1$ radiation (Ge-monochromated).

Experiment (i): powder XRD data were recorded on the impregnated powder sample at ambient temperature (294 K).

Experiment (ii): the impregnated powder sample was loaded into a capillary, which was quenched rapidly in liquid nitrogen; after quenching, the capillary was transferred to the powder XRD instrument and powder XRD data were recorded at ambient temperature (294 K). The aim of quenching was to mimic the experimental conditions of the DNP NMR studies.

To ensure that the powder XRD data of acceptable quality could be recorded as quickly as possible after quenching process in experiment (ii), the data were recorded only over the $2\theta$ range from 16° to 18°. Within this range, diagnostic peaks characteristic of Form I and Form III of *m*-ABA allow the presence or absence of each polymorph within the powder sample to be established.

As shown in Figure S1, the powder XRD data recorded in experiments (i) and (ii) are consistent with the presence of Form I of *m*-ABA, but show no evidence for the presence of Form III of *m*-ABA within the detection limit of the measurement.

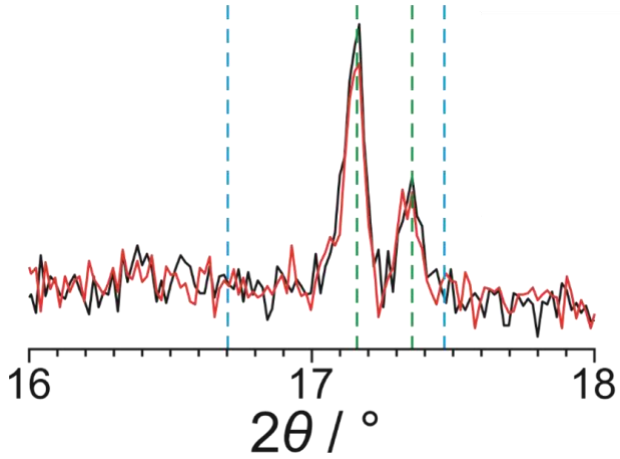


**Fig. S1:** Powder XRD data recorded at 294 K on a freshly prepared powder sample of Form I of *m*-ABA after impregnation with a solution of TEKPol in 1,1,2,2-tetrachloroethane. Black: powder XRD data recorded in experiment (i). Red: powder XRD data recorded in experiment (ii). Within the data range from $2\theta$ = 16° to 18°, diagnostic peaks for Form I of *m*-ABA occur at $2\theta$ = 17.16° and 17.36° (peak positions indicated by green dashed lines) and diagnostic peaks for Form III of *m*-ABA occur at $2\theta$ = 16.70° and 17.47° (peak positions indicated by blue dashed lines).

Powder XRD studies were also carried out before and after impregnating a freshly prepared powder sample of Form I of *m*-ABA with a solution containing AMUPol in glycerol-$D_2O$ (60/40 v/v), using the impregnation procedure described in the Methods section. The powder XRD data were recorded at ambient temperature (298 K) using a Rigaku RU-200BH instrument with a high-brightness copper anode (CuKα radiation; $\lambda$ = 1.5418 Å; beam size, 0.5 × 0.5 $mm^2$), a double reflection focusing optic (OSMIC) and a Mar345 type 2D detector.

As shown in Figure S2, the powder XRD data recorded before and after impregnation are essentially identical to each other and are characteristic of Form I of *m*-ABA, with no evidence for the presence of Form III of *m*-ABA within the detection limit of the measurement. We note that the peaks for Form I at $2\theta \approx 17.16°$ and $2\theta \approx 17.36°$ are not resolved in Figure S2, whereas they are resolved in the powder XRD data shown in Figure S1 as a consequence of the higher resolution of the instrument used to record the powder XRD data in Figure S1.

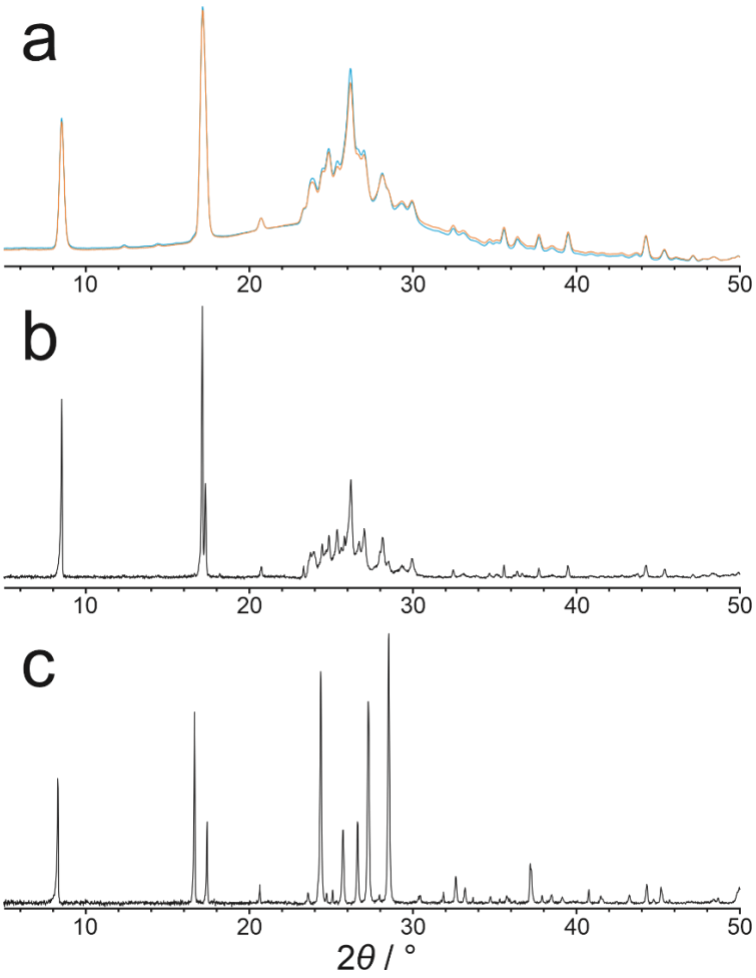


**Fig. S2:** (a) Powder XRD data recorded at 298 K for a freshly prepared powder sample of Form I of *m*-ABA before (blue) and after (orange) impregnation with a solution of AMUPol in glycerol-$D_2O$ (60/40 v/v). (b) Powder XRD data reported previously[1] for a monophasic sample of Form I of *m*-ABA. (c) Powder XRD data reported previously[1] for a monophasic sample of Form III of *m*-ABA. We note that the instrumental resolution of the powder X-ray diffractometer used to record the powder XRD data in (b) and (c) was significantly higher than the instrumental resolution of the powder X-ray diffractometer used to record the powder XRD data in (a).

## 1.2 Solid-state $^{13}C$ NMR Spectra Recorded at Different DNP Polarization Times for a Powder Sample of Form I of m-ABA Impregnated with AMUPol/glycerol-$D_2O$ Solution

$^{1}H$-$^{13}C$ CPMAS saturation recovery data recorded at different values of polarization time $\tau$ for a powder sample of Form I of *m*-ABA impregnated with a solution containing AMUPol in glycerol-$D_2O$ (60/40 v/v) are shown in Figure S3. The difference spectrum obtained by subtracting the spectrum recorded with $\tau$ = 10 s from the spectrum recorded with $\tau$ = 150 s exhibits the spectral features characteristic of Form III of *m*-ABA. This observation is identical to the results in Figure 1 of the main paper for the same type of experiment (although involving longer values of the polarization time $\tau$) on a powder sample of Form I of *m*-ABA impregnated with a solution containing TEKPol in 1,1,2,2-tetrachloroethane.

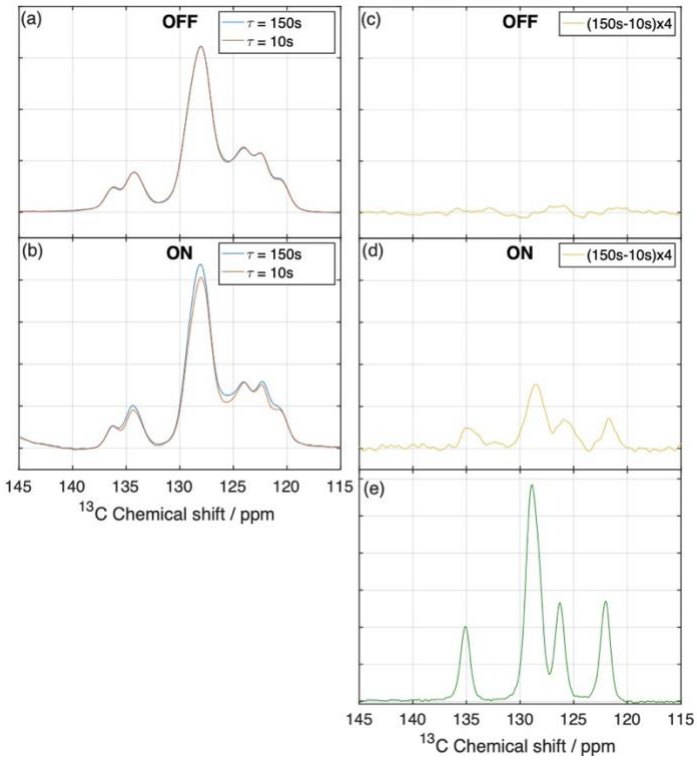


**Fig. S3:** Solid-state $^{13}$C NMR spectra recorded at 110 K for a powder sample of Form I of *m*-ABA impregnated with a solution containing AMUPol in glycerol-$D_2O$ (60/40 v/v) using the $^{1}$H-$^{13}$C CPMAS saturation-recovery pulse sequence at different values of polarization time $\tau$. The solid-state $^{13}$C NMR spectra were recorded (a, c) in the absence and (b, d) in the presence of microwave irradiation. In each case, the spectrum recorded with $\tau$ = 10 s is shown in red, the spectrum recorded with $\tau$ = 150 s is shown in blue, and the difference spectrum obtained by subtracting the spectrum recorded with $\tau$ = 10 s from the spectrum recorded with $\tau$ = 150s is shown in orange. For comparison, the solid-state $^{13}$C NMR spectrum of a pure sample of Form III of *m*-ABA is shown in green (e).

## 1.3 Solid-state $^{13}$C NMR Signal Intensities as a Function of DNP Polarization Time for a Powder Sample of Form I of m-ABA Impregnated with TEKPol/$EtCl_4$ Solution

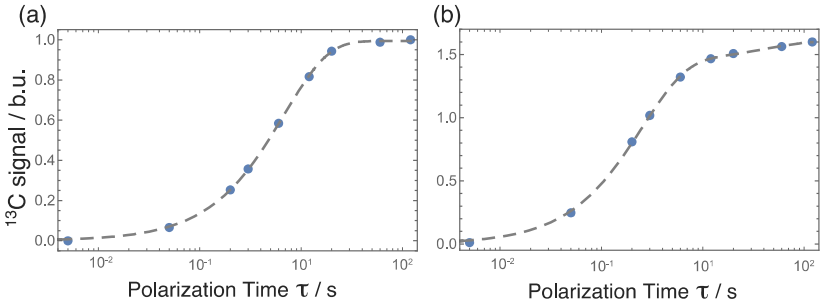


**Fig. S4:** Experimental $^{13}$C NMR signal intensity as a function of polarization time $\tau$ for a sample of Form I of *m*-ABA impregnated with the TEKPol/$EtCl_4$ solution. The data were recorded using the $^{1}$H-$^{13}$C CPMAS saturation recovery pulse sequence either (a) with no microwave irradiation applied or (b) with microwave irradiation applied. Exponential fits of the experimental data are shown with dashed lines. In (a), the experimental data show a mono-exponential buildup curve with $T_{B,OFF}$ = 6.8 s. In (b), the experimental data show a bi-exponential buildup curve with $T_{B,ON}(1)$ = 2.5 s and $T_{B,ON}(2)$ = 42 s. The signals are normalized to Boltzmann units (b.u.), where one Boltzmann unit is the polarization level reached without DNP or depolarization effects.

## 1.4 Solid-state $^{13}$C NMR Signal Intensities as a Function of DNP Polarization Time for a Sample of m-ABA Dissolved in AMUPol/DMSO Solution

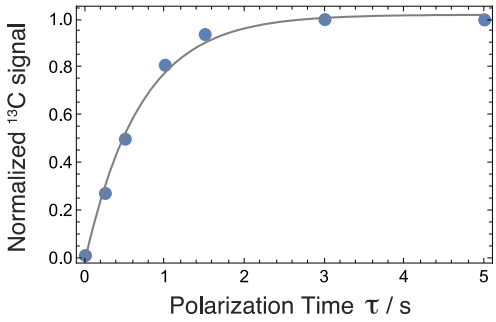


**Fig. S5:** Experimental $^{13}$C NMR signal intensity of *m*-ABA as a function of polarization time $\tau$ for a sample consisting of 9 mg of Form I of m-ABA as a powder dissolved in a solution (12 mM; 100 µl) containing AMUPol dissolved in DMSO. The data were recorded at 100 K using the $^{1}$H-$^{13}$C CPMAS saturation recovery pulse with microwave irradiation applied (signals are not expressed in Boltzmann units here because the $^{13}$C NMR signals of *m*-ABA could not be detected in the spectrum recorded with no microwave irradiation applied). The line shows the fit to the experimental data using a mono-exponential build-up curve with build-up time $T_{B,ON}$ = 0.70 ± 0.1 s.

## 1.5 Solid-state $^{13}$C NMR spectra of m-ABA as a powder or as a frozen solution

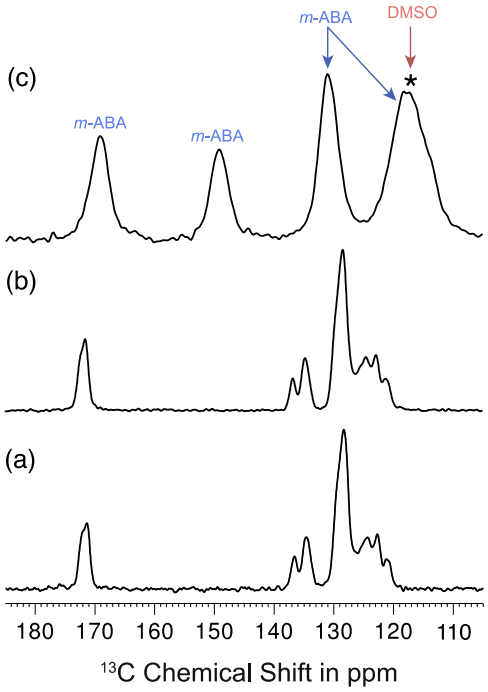


**Fig. S6:** Solid-state $^{13}$C NMR spectra recorded at 100 K for: (a) a powder sample of Form I of *m*-ABA, (b) a powder sample of Form I of *m*-ABA following impregnation with TEKPol/$EtCl_4$ solution (20 µl), and (c) the "frozen solution" obtained by quenching (to 100 K) a solution prepared by dissolving a powder sample of Form I of *m*-ABA (9 mg) in a solution (12 mM; 100 µl) containing AMUPol dissolved in DMSO. The data were recorded using the $^{1}$H-$^{13}$C CPMAS saturation recovery pulse sequence with no microwave irradiation applied in (a) and (b), and with microwave irradiation applied in (c). In (c), the peak marked * represents the overlap of a $^{13}$C resonance of *m*-ABA and a spinning sideband from the $^{13}$C resonance of DMSO.

### 1.6 Build-up time of the $^{13}C$ NMR Signal at 137 ppm as a Function of DNP Polarization Time for a Powder Sample of Form I of m-ABA

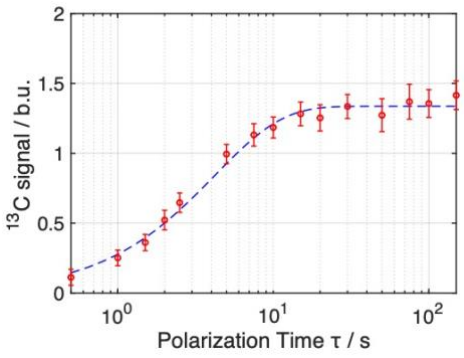


**Fig. S7:** Experimental build-up curves (data points with error bars) for the $^{13}C$ resonance at 137 ppm for a powder sample of Form I of m-ABA impregnated with AMUPol/glycerol-$D_2O$ solution, Experimental data were recorded using $^{1}H$-$^{13}C$ CPMAS saturation recovery as a function of polarization time $\tau$ with microwave irradiation applied. Fits to the experimental data are shown by dashed lines. The experimental data in (a) are described by a mono-exponential build-up curve with build-up time $T_{B,ON}$ = 4 s. The dashed line shows the fit to the experimental data using a mono-exponential build-up curve with build-up time $T_{B,ON}$ = 4 s. Signals are expressed in Boltzmann units (b.u.).

## 2. Numerical Simulations for Models A – E Based on Well-Defined Spatial Distributions of Polymorphic Phases within Particles in a Powder Sample

### 2.1 Model B (distinct particles of pure Form I and pure Form III)

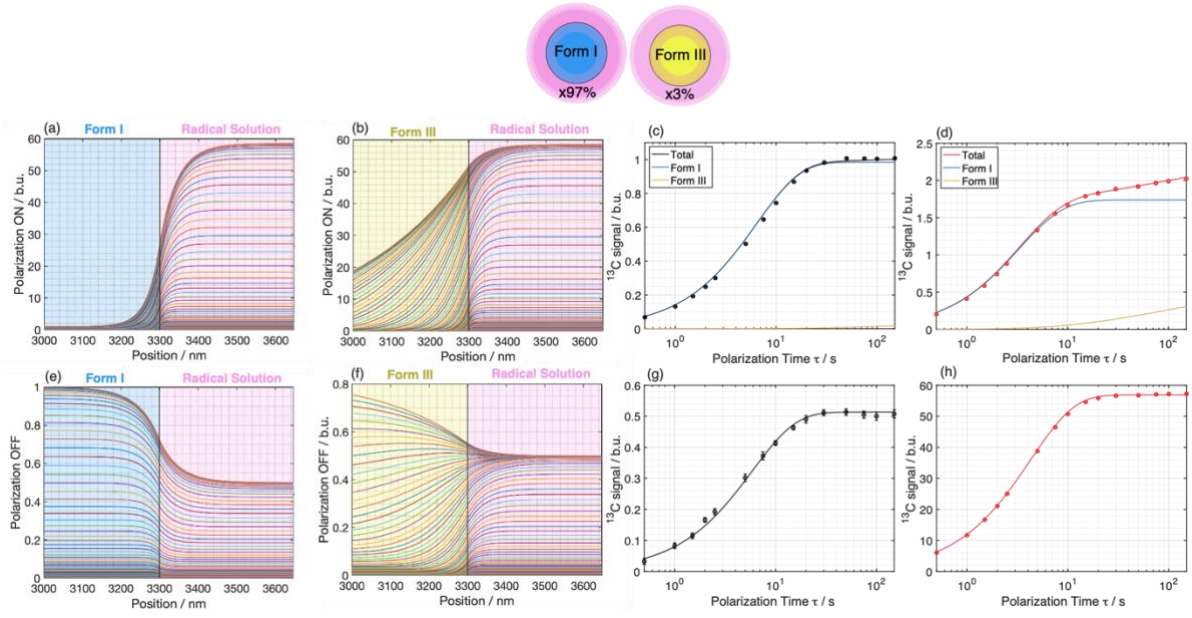


**Fig. S7:** Results for Model B in which 3% of the spherical particles are pure Form III and 97% of the spherical particles are pure Form I. Simulations of radial polarization as a function of the position near the surface of the particle: (a, b) in the presence and (e, f) in the absence of microwave irradiation for polarization times ranging from $\tau$ = 0.5 to 150 s in exponential steps. Experimental (• or •) build-up curves (c, d) for a powder sample of Form I of *m*-ABA impregnated with AMUPol/glycerol-$D_2O$ solution and (g, h) the AMUPol/glycerol-$D_2O$ solution (g, h). Experimental data were recorded using $^{1}H$-$^{13}C$ CPMAS saturation recovery as a function of polarization time $\tau$, either (d, h) with or (c, g) without microwave irradiation. The solid lines (— or —) indicate the best-fit simulated build-up curves with (c) and (d) also showing the best-fit

simulated build-up curves simulated for the particles of Form I (blue solid line) and the particles of Form III (yellow solid line). The best agreement is obtained for 3% of Form III and 97% of Form I, and with radius $R$ = 3.3 μm for each type of particle.

The distribution of the polymorphic phases in Model B comprises distinct particles of pure Form I and pure Form III. Results for this model are shown in Figure S5. In addition, Figure S5c and S5d also show the individual best-fit build-up curves simulated for the individual particles of Form I and Form III.

An excellent agreement between the experimental and simulated build-up curves is obtained for model B, either in the absence or in the presence of microwave irradiation. It should be noted that both simulated build-up curves have a bi-exponential behavior, although the build-up curve simulated in absence of microwave cannot be distinguished from a mono-exponential buildup curve and thus the minor polymorphic form cannot be identified in this case. On the other hand, the build-up curve simulated in presence of microwave is clearly bi-exponential, allowing the presence of the minor polymorphic form to be unambiguously established.

## 2.2 Model C (core-shell particles with Form III in the shell)

In Model C, Form III is present in the outer shell of each particle, with the core of the particle containing Form I. Results for this model are shown in Figure S6.

From Figure S6(b), we deduce that the fraction of Form III cannot be greater than 5%, as Form III would be detected even without DNP, leading to a bi-exponential build-up curve. From the magnitude of the enhancement in Figure S1c, the particle radius is determined to be $R$ = 7 μm, as smaller particles would give a higher enhancement, and *vice versa*.

Knowing an upper limit for the fraction of Form III present in the sample and the particle size, the thickness of the shell of Form III in this model is 70 nm, corresponding to 3% of Form III. In this system, the thickness of the shell of Form III is much less than the spin diffusion length of Form III, meaning that spin diffusion is very efficient in accelerating the build-up for Form III. In the present case, the accelerated build-up for Form III would be roughly equal to the non-accelerated build-up for Form I, which would lead to a mono-exponential build-up curve. As a bi-exponential build-up curve is observed experimentally, core-shell Model C can be ruled out.

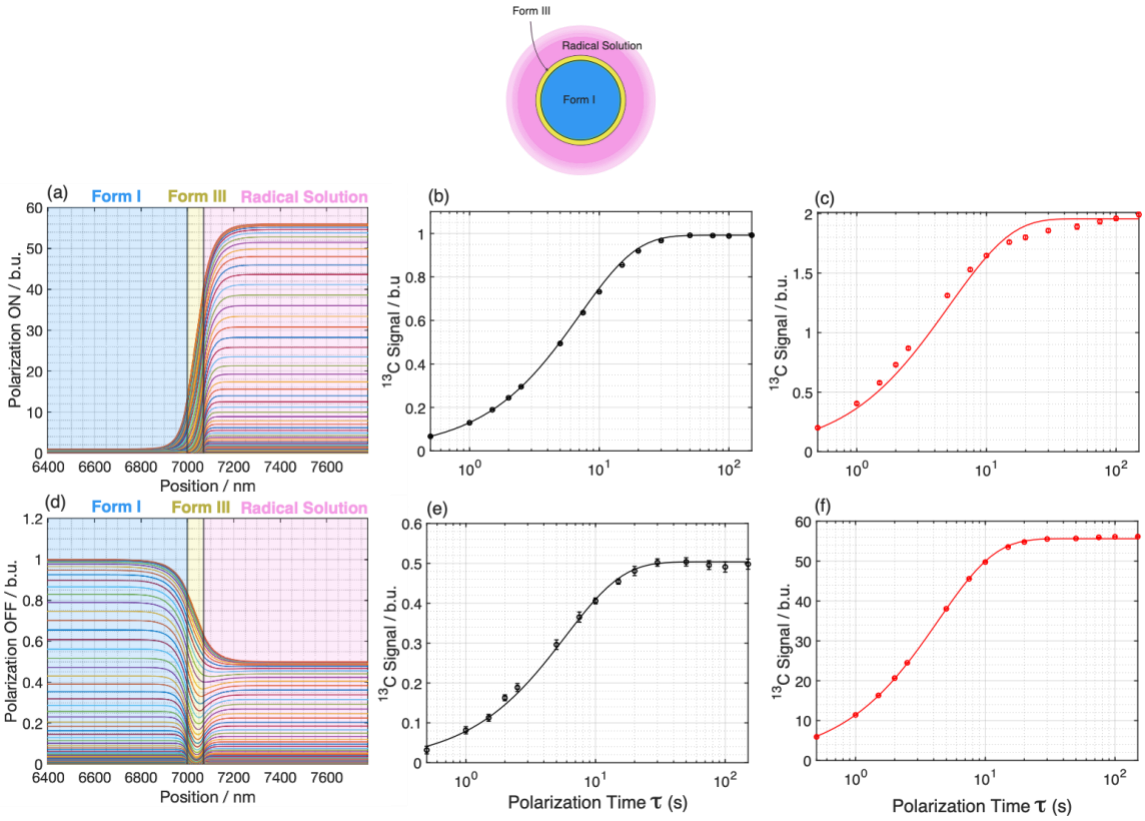


**Fig. S8:** Results for Model C, the core-shell model for a spherically symmetric particle in which Form III is present in the outer shell and Form I is present in the spherical core. Simulations of radial polarization as a function of position near the surface of the particle (a) in the presence and (d) in the absence of microwave irradiation for polarization times ranging from $\tau$ = 0.5 s to 150 s in exponential steps. Experimental (• or •) build-up curves for (b, c) a powder sample of Form I of *m*-ABA impregnated with AMUPol/glycerol-$D_2O$ solution and (e, f) the AMUPol/glycerol-$D_2O$ solution. Experimental data were recorded either with (c, d) or without (a, b) microwave irradiation. The solid lines (— or —) indicate the best-fit simulated build-up curves. The best agreement is obtained for particles of radius $R$ = 7.07 μm containing 3% of Form III and 97% of Form I, as shown in (c), although the agreement is not perfect, with a deviation observed between the simulated and experimental build-up curves.

## 2.3 Model E (Form III embedded as a region extending from the surface to the core of particles of Form I)

This model is based on spherical particles of Form I, with a conical region of Form III embedded within each particle (see Figure 3 in main paper). The apex of the conical region of Form III is at the center of the spherical particle and the base of the conical region of Form III is at the surface of the spherical particle.

As shown in Figure S7, the best agreement between experimental and simulated build-up curves is obtained for a particle radius of $R$ = 4.6 μm, and with a composition comprising 96% of Form I and 4% of Form III.

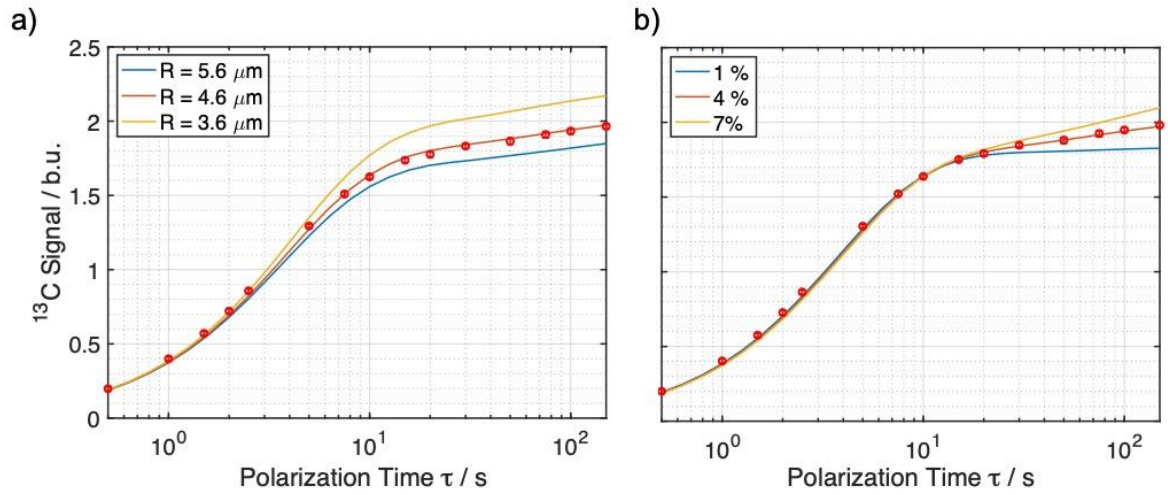


**Fig. S9:** Experimental (•) and simulated (solid lines) build-up curves calculated for Model E under microwave irradiation using (a) 4% of Form III and different values of the radius *R* of the spherical particles and (b) different values of the percentage of Form III and *R* = 4.6 μm.

# References

[1] P. A. Williams, C. E. Hughes, G. K. Lim, B. M. Kariuki, K. D. M. Harris, *Cryst. Growth Des.* **2012**, *12*, 3104.